Journal of System Design and Dynamics

Vol. 1, No. 3, 2007

A Study of Vibration Control Systems for Superconducting Maglev Vehicles

(Vibration Control of Lateral and Rolling Motions)*

Ken WATANABE**, Hiroshi YOSHIOKA***, Erimitsu SUZUKI**, Takayuki TOHTAKE** and Masao NAGAI****

**Railway Technical Research Institute,
2-8-38 Hikari-cho, Kokubunji-shi, Tokyo, Japan
E-mail: ken_w@rtri.or.jp

***Central Japan Railway Co., Ltd.,
JR Central Shinagawa Bldg., A-Wing, 2-1-85 Konan, Minato-ku, Tokyo, Japan

****Tokyo University of Agriculture and Technology,
2-24-16 Naka-cho, Koganei-shi, Tokyo, Japan

Abstract

The superconducting magnetically levitated transport (Maglev) system is conceptualized as a next-generation high-speed transportation system. For practical use, it is important to achieve adequate ride comfort particularly in high-speed running. Maglev vehicles are composed of lightweight car bodies and relatively heavy bogies which are mounted with devices such as superconducting magnets (SCMs) and an on-board refrigerating system. In this magnetically levitated system, the passive electromagnetic damping in the primary suspension between the SCMs and ground coils is very small. Therefore, it is effective to add active electromagnetic damping to this primary suspension, and to adjust the secondary suspension between the car body and bogie. This paper examines vibration control systems of the Maglev vehicle using actuators for the secondary suspension. Moreover, the estimated electromagnetic damping, which interacts between the SCMs and the guideway, is also considered in the model to improve the ride comfort.

Key words: Railway, Vibration Control, Electromagnetically Induced Vibration, Ride Comfort

1. Introduction

The superconducting magnetically levitated transport (Maglev) system is a promising future mode of mass transit. In the efforts toward the realization of commercial operation, costs are a major issue as well as the attainment of ride comfort suitable for a public mode of transportation. Moreover, in order to reduce running costs such as of the propulsion energy consumption and guideway maintenance, reducing the weight of Maglev vehicles is very important. On the other hand, the reduction in car body weight tends to worsen the ride comfort with respect to vibration, and is disadvantageous in terms of vibration isolation. Specifically, passive damping between the superconducting magnets (SCMs) and ground coils is not expected to be significantly large in this superconducting Maglev system.

In this paper, applications of vibration control systems to Maglev vehicles were examined as a means to improve ride comfort. The future is bright for vibration control applications on Maglev vehicles if the methods effectively improve ride comfort, and if the

*Received 6 Mar., 2007 (No. T1-03-1168)
Japanese Original : Trans. Jpn. Soc. Mech. Eng., Vol. 71, No. 701, C (2005), pp.114-121 (Received 14 Oct., 2003)
[DOI: 10.1299/jsdd.1.593]

reduction of construction costs by relaxing the limits of tolerated irregularities in the guideway alignment and the reduction of management costs by minimizing guideway maintenance exceeds the increase in vehicle costs due to installation of vibration control systems.

This paper focuses on a fundamental investigation of the improvement of ride comfort in Maglev vehicles with respect to lateral and rolling motions, and simulations were performed to confirm the theoretical effectiveness of vibration control methods.

2. Computation Model

2.1 Overview of the computation model

In railway vehicles, the frequency range that most greatly influences ride comfort with respect to lateral motion is known to be relatively low. In contrast, because Maglev vehicles travel at high speeds of approximately 500 km/h, errors in the alignment of the guideway structure (guideway irregularities) that are a source of disturbances are characterized by waveforms with wavelengths longer than the length of a car body of a Maglev vehicle, and the component of the car body longitudinal vibration mode in this frequency range is not that large. Therefore, this paper mainly focuses on fundamental examinations of the improvement of ride comfort with respect to lateral and rolling motions in ordinary vehicle runs, using a cross-sectional model consisting of a car body and bogie with lateral and rolling motions resulting in four degrees of freedom, as shown in Fig. 1.[(1)(2)]

Using vehicle specifications from Refs. (3) and (4), the intermediate bogie mass and the corresponding car body equivalent mass were determined. The equivalent moment of inertia was derived from the equivalent mass and the height of the center of mass. The secondary suspension of Maglev vehicles consist of air springs and vertical and lateral dampers that connect the car body and bogie, similar to conventional railway vehicles. Air springs and dampers with ideal characteristics were used in the computation model. Furthermore, the primary suspension consisting of electromagnetic interactions between the superconducting magnet (SCM) and the levitation-guidance coils on the guideway were modeled using springs with linear characteristics for lateral and rolling motions. The guideway irregularities were assumed to generate disturbances in the primary suspension resulting in vibrations in the vehicle, and aerodynamic effects were assumed to be negligible. Guideway

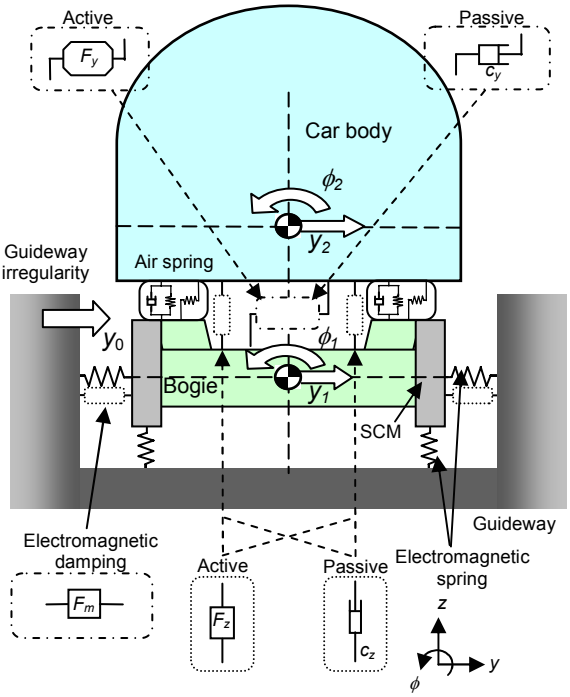

Fig. 1 Four-degree-of-freedom computation model

irregularities in the lateral direction (lateral irregularities) were assumed to be dominant. Therefore, guideway irregularities in the rolling direction were omitted, and only lateral irregularities were considered.

In Maglev systems, the magnetic springs in the lateral and rolling directions are strongly coupled with each other.[3] In other words, a lateral displacement of the vehicle results in a lateral restoring force as well as a rolling moment. This coupled spring has also been incorporated into the model.

2.2 Dynamic equations

Dynamic equations were derived for the passive model of Fig. 1 which includes dampers in the vertical and lateral directions in the secondary suspension. The major symbols used in the equations are as follows:

m_1, m_2: masses
I_1, I_2: moments of inertia
k_{py}, k_{pz}: spring constants of air springs per bogie
c_y, c_z: damping coefficients of dampers per bogie
h_{a1}, h_{a2}: air spring attachment heights
h_{c1}, h_{c2}: lateral damper attachment heights
b_a: half of the lateral distance between attachment points of air springs
b_c: half of the lateral distance between attachment points of vertical dampers
k_{myy}, $k_{my\phi}$, $k_{m\phi y}$, $k_{m\phi\phi}$: spring constants of magnetic springs per bogie
y_1, y_2: lateral displacements
ϕ_1, ϕ_2: rolling-angular displacements
y_0: guideway lateral irregularities

The subscript "*1*" denotes the bogie, and "*2*" denotes the car body. The spring constants of the magnetic springs k_{mij} have been derived from forces and moments acting in the i direction resulting from translational and angular displacements in the j direction. The attachment heights are based on measurements from mass centers of the car body and bogie.

Using the aforementioned symbols, dynamic equations of the passive model are expressed as follows:

Bogie lateral motion

$$\begin{aligned} & m_1 \cdot \ddot{y}_1 + k_{py}\left\{\left(y_1 - y_2\right) - \left(h_{a1} \cdot \phi_1 + h_{a2} \cdot \phi_2\right)\right\} \\ & \quad + c_{dy}\left\{\left(\dot{y}_1 - \dot{y}_2\right) - \left(h_{c1} \cdot \dot{\phi}_1 + h_{c2} \cdot \dot{\phi}_2\right)\right\} \\ & \quad + k_{myy} \cdot y_1 + k_{my\theta} \cdot \phi_1 = k_{myy} \cdot y_0 \end{aligned} \tag{1}$$

Bogie rolling motion

$$\begin{aligned} & I_1 \cdot \ddot{\phi}_1 + k_{py} \cdot h_{a1}\left\{\left(y_2 - y_1\right) + \left(h_{a1} \cdot \phi_1 + h_{a2} \cdot \phi_2\right)\right\} \\ & \quad + c_{dy} \cdot h_{c1}\left\{\left(\dot{y}_2 - \dot{y}_1\right) + \left(h_{c1} \cdot \dot{\phi}_1 + h_{c2} \cdot \dot{\phi}_2\right)\right\} \\ & \quad + k_{pz} \cdot b_a^{\,2}\left(\phi_1 - \phi_2\right) + c_{dz} \cdot b_c^{\,2}\left(\dot{\phi}_1 - \dot{\phi}_2\right) \\ & \quad + k_{m\phi\phi} \cdot \phi_1 = k_{m\phi y} \cdot y_0 \end{aligned} \tag{2}$$

Car body lateral motion

$$\begin{aligned} & m_2 \cdot \ddot{y}_2 + k_{py}\left\{\left(y_2 - y_1\right) + \left(h_{a2} \cdot \phi_2 + h_{a1} \cdot \phi_1\right)\right\} \\ & \quad + c_{dy}\left\{\left(\dot{y}_2 - \dot{y}_1\right) + \left(h_{c2} \cdot \dot{\phi}_2 + h_{c1} \cdot \dot{\phi}_1\right)\right\} = 0 \end{aligned} \tag{3}$$

Car body rolling motion

$$\begin{aligned} & I_2 \cdot \ddot{\phi}_2 + k_{py} \cdot h_{a2}\left\{\left(y_2 - y_1\right) + \left(h_{a1} \cdot \phi_1 + h_{a2} \cdot \phi_2\right)\right\} \\ & \quad + c_{dy} \cdot h_{c2}\left\{\left(\dot{y}_2 - \dot{y}_1\right) + \left(h_{c1} \cdot \dot{\phi}_1 + h_{c2} \cdot \dot{\phi}_2\right)\right\} \\ & \quad + k_{pz} \cdot b_a^{\,2}\left(\phi_2 - \phi_1\right) + c_{dz} \cdot b_c^{\,2}\left(\dot{\phi}_2 - \dot{\phi}_1\right) = 0 \end{aligned} \tag{4}$$

The state variables of this model are:

$$x = \begin{bmatrix} y_1 & \dot{y}_1 & y_2 & \dot{y}_2 & \phi_1 & \dot{\phi}_1 & \phi_2 & \dot{\phi}_2 \end{bmatrix}^T \tag{5}$$

The state equation is expressed as:

$$\dot{x} = Ax + Wy_0 \tag{6}$$

The system matrix A is defined as:

$$A = \begin{bmatrix} 0 & 1 & 0 & 0 & 0 & 0 & 0 & 0 \\ a_{21} & a_{22} & a_{23} & a_{24} & a_{25} & a_{26} & a_{27} & a_{28} \\ 0 & 0 & 0 & 1 & 0 & 0 & 0 & 0 \\ a_{41} & a_{42} & a_{43} & a_{44} & a_{45} & a_{46} & a_{47} & a_{48} \\ \vdots & \vdots & \vdots & \vdots & \vdots & \vdots & \vdots & \vdots \\ a_{81} & a_{82} & a_{83} & a_{84} & a_{85} & a_{86} & a_{87} & a_{88} \end{bmatrix} \tag{7}$$

The elements of this matrix are as follows:

$$\begin{aligned}
a_{21} &= -\left(k_{myy} + k_{py}\right)/m_1 & a_{22} &= -c_{dy}/m_1 \\
a_{23} &= k_{py}/m_1 & a_{24} &= c_{dy}/m_1 \\
a_{25} &= \left(h_{a1} \cdot k_{py} - k_{my\phi}\right)/m_1 & a_{26} &= h_{c1} \cdot c_{dy}/m_1 \\
a_{27} &= h_{a2} \cdot k_{py}/m_1 & a_{28} &= h_{c2} \cdot c_{dy}/m_1 \\
a_{41} &= k_{py}/m_2 & a_{42} &= c_{dy}/m_2 \\
a_{43} &= -k_{py}/m_2 & a_{44} &= -c_{dy}/m_2 \\
a_{45} &= -h_{a1} \cdot k_{py}/m_2 & a_{46} &= -h_{c1} \cdot c_{dy}/m_2 \\
a_{47} &= -h_{a2} \cdot k_{py}/m_2 & a_{48} &= -h_{c2} \cdot c_{dy}/m_2 \\
a_{61} &= \left(h_{a1} \cdot k_{py} - k_{my\phi}\right)/I_1 & a_{62} &= h_{c1} \cdot c_{dy}/I_1 \\
a_{63} &= -h_{a1} \cdot k_{py}/I_1 & a_{64} &= -h_{c1} \cdot c_{dy}/I_1 \\
a_{65} &= -\left(b_a^2 \cdot k_{pz} + h_{a1}^2 \cdot k_{py} + k_{m\phi\phi}\right)/I_1 & a_{66} &= -\left(b_c^2 \cdot c_{dz} + h_{c1}^2 \cdot c_{dy}\right)/I_1 \\
a_{67} &= \left(b_a^2 \cdot k_{pz} - h_{a1} \cdot h_{a2} \cdot k_{py}\right)/I_1 & a_{68} &= \left(b_c^2 \cdot c_{dz} - h_{c1} \cdot h_{c2} \cdot c_{dy}\right)/I_1 \\
a_{81} &= h_{a2} \cdot k_{py}/I_2 & a_{82} &= h_{c2} \cdot c_{dy}/I_2 \\
a_{83} &= -h_{a2} \cdot k_{py}/I_2 & a_{84} &= -h_{c2} \cdot c_{dy}/I_2 \\
a_{85} &= \left(b_a^2 \cdot k_{pz} - h_{a1} \cdot h_{a2} \cdot k_{py}\right)/I_2 & a_{86} &= \left(b_c^2 \cdot c_{dz} - h_{c1} \cdot h_{c2} \cdot c_{dy}\right)/I_2 \\
a_{87} &= -\left(b_a^2 \cdot k_{pz} + h_{a2}^2 \cdot k_{py}\right)/I_2 & a_{88} &= -\left(b_c^2 \cdot c_{dz} + h_{c2}^2 \cdot c_{dy}\right)/I_2
\end{aligned}$$

The external disturbance matrix W is expressed as:

$$W = \begin{bmatrix} 0 & k_{myy}/m_1 & 0 & 0 & 0 & k_{m\phi y}/I_1 & 0 & 0 \end{bmatrix}^T \tag{8}$$

The parameters used in the computations are shown in Table 1.

Table 1 Computation parameters

Symbol (unit)	Value	Symbol (unit)	Value
m_1 (kg)	6.0×10^3	m_2 (kg)	14.0×10^3
I_1 $(kg\cdot m^2)$	9.5×10^3	I_2 $(kg\cdot m^2)$	21.5×10^3
k_{py} (N/m)	0.6×10^6	k_{pz} (N/m)	0.8×10^6
c_y $(N\cdot s/m)$	50.0×10^3	c_z $(N\cdot s/m)$	40.0×10^3
h_{a1} (m)	0.85	h_{a2} (m)	0.35
h_{c1} (m)	0.85	h_{c2} (m)	0.35
b_a (m)	1.15	b_c (m)	1.15
k_{myy} (N/m)	3.1×10^6	$k_{m\phi y}$ (N)	-4.2×10^6
$k_{m\phi\phi}$ $(N\cdot m/rad)$	10.4×10^6	$k_{my\phi}$ (N)	-4.2×10^6

2.3 Characteristics of the passive case

(1) Frequency responses

In the passive model of Fig. 1, a sine wave with a magnitude of 1 mm was used as input for

the guideway lateral irregularities, and frequency responses of accelerations were computed for a vehicle traveling at 500 km/h. The computation results of car body lateral and rolling-angular accelerations are shown in Fig. 2. In this figure, two large peaks are noticeable for the car body lateral acceleration, at around 1 to 2.5 Hz and at around 6.5 Hz. The absolute value of the acceleration of the peak at the higher frequency range is larger than the peak at the lower frequency range. This higher frequency range is within the region that is known to be relatively insensible by human perception, according to frequency weighting curves for lateral motions defined by ISO-2631 (guide for evaluation of human exposure to whole-body vibration). Therefore, the ride comfort with respect to vehicle vibrations is presumed to be more greatly influenced by the vibration peak at around 1 to 2.5 Hz than by the peak at around 6.5 Hz. As shown in Fig. 2, three large peaks of the car body rolling-angular acceleration exist at around 1 Hz, 2.5 Hz, and 6.5 Hz, and the differences in the absolute heights of these peaks are very small.

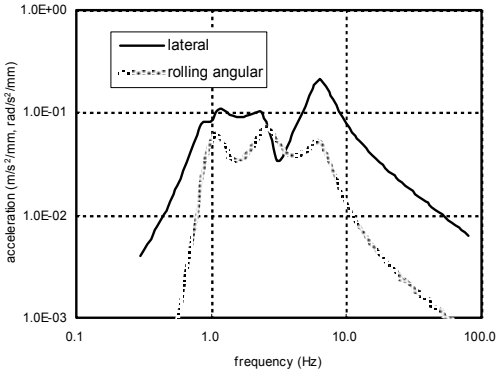

Fig. 2 Frequency responses of car body lateral and roll angular acceleration of passive model

Table 2 Eigenvalues and eigenvectors of the passive model

Eigenvalue (Hz)		Eigenvector			
		y_1	y_2	ϕ_1	ϕ_2
1st	0.876	0.053	0.870	-0.051	-0.453
2nd	1.053	0.391	0.553	0.188	0.695
3rd	2.561	0.883	-0.112	0.432	-0.132
4th	6.429	-0.611	0.034	0.790	-0.016

(2) Eigenvalues and mode eigenvectors

Setting the damping coefficients to zero in the vertical and lateral dampers between the car body and bogie of the passive model in Fig. 1, the eigenvalues and mode eigenvectors were computed, and the shapes of the vibration modes were examined. The eigenvalues and mode eigenvectors are shown in Table 2, and the shapes of the vibration modes are shown in Fig. 3. The same figure shows that in the first mode (0.876 Hz), the car body and bogie swing together in nearly the same phase in a rolling motion with the center of rotation in the lower part of the vehicle, resembling an inverted pendulum. The bogie vibration amplitude is very small, and the car body motion is predominant in this mode. The second mode (1.053 Hz) is characterized by the car body and bogie swinging together in nearly the same phase in a rolling motion with the center of rotation in the upper part of the vehicle, resembling an upright pendulum. In the third mode (2.561 Hz), the car body and bogie swing in opposite phases in rolling motions with the rotation center in the upper part of the vehicle. The car body vibration amplitude is very small, and bogie motion is predominant in

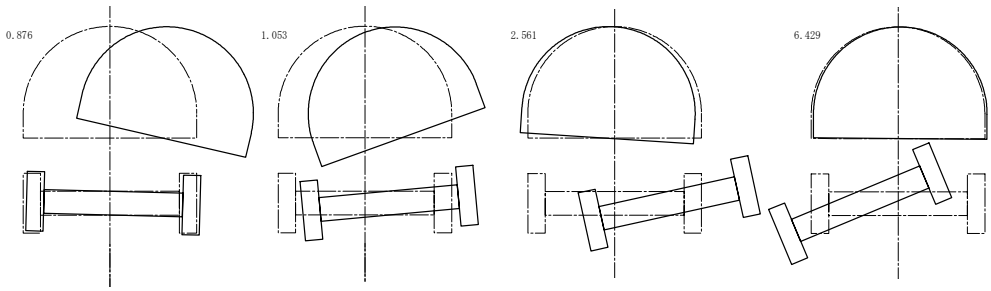

Fig. 3 Vibration modes of passive model

this mode. The fourth mode (6.429 Hz) is characterized by car body lateral motion and bogie rolling motion with the rotation center in the lower part of the vehicle.

3. Vibration Control Systems

3.1 Control systems

In this paper, the following two methods of improving ride comfort were examined:

(a) the case in which active suspension in the lateral and rolling directions using linear quadratic (LQ) control is applied to the secondary suspension

(b) the case in which active suspension is applied to the secondary suspension, combined with lateral motion damping force control in the primary suspension using electromagnetic forces output by a linear generator integrated into the bogie

Based on the results of vibration mode analyses in the previous chapter, the vibration control of the secondary suspension is expected to be directed mainly to the first and second modes, and the control of the primary suspension directed mainly to the third mode. Details of these methods of control are described hereinafter.

3.2 Vibration control of the secondary suspension[5]

In the control of the secondary suspension, the vertical and lateral dampers were replaced by actuators, and the effectiveness of vibration control of lateral and rolling motions were examined. In this paper, two types of control methods are examined. In Type 1, only the lateral dampers were replaced by actuators, to control lateral motion. In Type 2, vertical actuators were also used, to control the rolling motion in addition to lateral motion. The control systems were designed using the forces generated by these actuators as control input. Furthermore, these actuators were assumed to be ideal with no delay in response. As an example, the derivations of the dynamic equations of the control of lateral and rolling motions (Type 2) are shown hereinafter. The dynamic equations including the control force are shown below in Eqs. (9) ~ (12), with u representing the control force, the subscript "l" representing the lateral direction, and the subscript "v" representing the rolling direction.

Bogie lateral motion

$$\begin{aligned} & m_1 \cdot \ddot{y}_1 + k_{py}\left\{\left(y_1 - y_2\right) - \left(h_{a1} \cdot \phi_1 + h_{a2} \cdot \phi_2\right)\right\} \\ & \quad + c_{dy}\left\{\left(\dot{y}_1 - \dot{y}_2\right) - \left(h_{c1} \cdot \dot{\phi}_1 + h_{c2} \cdot \dot{\phi}_2\right)\right\} \\ & \quad + k_{myy} \cdot y_1 + k_{my\phi} \cdot \phi_1 = k_{myy} \cdot y_0 - u_l \end{aligned} \tag{9}$$

Bogie rolling motion

$$\begin{aligned} & I_1 \cdot \ddot{\phi}_1 + k_{py} \cdot h_{a1}\left\{\left(y_2 - y_1\right) + \left(h_{a1} \cdot \phi_1 + h_{a2} \cdot \phi_2\right)\right\} \\ & \quad + c_{dy} \cdot h_{c1}\left\{\left(\dot{y}_2 - \dot{y}_1\right) + \left(h_{c1} \cdot \dot{\phi}_1 + h_{c2} \cdot \dot{\phi}_2\right)\right\} \\ & \quad + k_{pz} \cdot b_a{}^2\left(\phi_1 - \phi_2\right) + c_{dz} \cdot b_c{}^2\left(\dot{\phi}_1 - \dot{\phi}_2\right) \\ & \quad + k_{m\phi\phi} \cdot \phi_1 = k_{m\phi y} \cdot y_0 + h_{c1} \cdot u_l - b_c \cdot u_v \end{aligned} \tag{10}$$

Car body lateral motion

$$\begin{aligned} & m_2 \cdot \ddot{y}_2 + k_{py}\left\{\left(y_2 - y_1\right) + \left(h_{a2} \cdot \phi_2 + h_{a1} \cdot \phi_1\right)\right\} \\ & \quad + c_{dy}\left\{\left(\dot{y}_2 - \dot{y}_1\right) + \left(h_{c2} \cdot \dot{\phi}_2 + h_{c1} \cdot \dot{\phi}_1\right)\right\} = u_l \end{aligned} \tag{11}$$

Car body rolling motion

$$\begin{aligned} & I_2 \cdot \ddot{\phi}_2 + k_{py} \cdot h_{a2}\left\{\left(y_2 - y_1\right) + \left(h_{a1} \cdot \phi_1 + h_{a2} \cdot \phi_2\right)\right\} \\ & \quad + c_{dy} \cdot h_{c2}\left\{\left(\dot{y}_2 - \dot{y}_1\right) + \left(h_{c1} \cdot \dot{\phi}_1 + h_{c2} \cdot \dot{\phi}_2\right)\right\} \\ & \quad + k_{pz} \cdot b_a{}^2\left(\phi_2 - \phi_1\right) + c_{dz} \cdot b_c{}^2\left(\dot{\phi}_2 - \dot{\phi}_1\right) = h_{c2} \cdot u_l + b_c \cdot u_v \end{aligned} \tag{12}$$

Based on the equations above and the control input matrix defined as B, the state

equation is expressed as follows:

$$\dot{x} = Ax + Bu + Wy_0 \tag{13}$$

The control input matrix B, is expressed in two forms as follows:

$$B = \begin{bmatrix} 0 \\ -1/m_1 \\ 0 \\ 1/m_2 \\ 0 \\ h_{c1}/I_1 \\ 0 \\ h_{c2}/I_2 \end{bmatrix} \tag{14}$$

$$B = \begin{bmatrix} 0 & 0 \\ -1/m_1 & 0 \\ 0 & 0 \\ 1/m_2 & 0 \\ 0 & 0 \\ h_{c1}/I_1 & -b_c/I_1 \\ 0 & 0 \\ h_{c2}/I_2 & b_c/I_2 \end{bmatrix} \tag{15}$$

Equation (14) expresses the matrix for control of lateral motion only, and Eq. (15) for control of rolling and lateral motions.

Next, secondary suspension control based on LQ theory was applied to the system defined by Eq. (13). The designated objective of the control is to reduce the lateral acceleration of the car body cabin floor (X_1) and the vertical accelerations that result from rolling motions of the ends of the car body (X_2). In the criteria function, weighting factors were included for X_1 and X_2. Furthermore, to ensure that the gap is sufficient to prevent contact between the bogie and guideway, weighting factors were also included for the lateral displacement between the SCM and guideway X_3, the vertical displacement between the bottom end of the SCM and the guideway X_4, and the actuator control force u.

The criteria functions for control of lateral motion only and for control of both lateral and rolling motions are shown in Eqs. (16) and (17), respectively.

$$J = \int_0^\infty \left(q_1 \cdot X_1^2 + q_2 \cdot X_2^2 + q_3 \cdot X_3^2 + q_4 \cdot X_4^2 + r \cdot u^2 \right) dt \tag{16}$$

$$J = \int_0^\infty \left(q_1 \cdot X_1^2 + q_2 \cdot X_2^2 + q_3 \cdot X_3^2 + q_4 \cdot X_4^2 + r_l \cdot u_l^2 + r_v \cdot u_v^2 \right) dt \tag{17}$$

Within these equations,

$$X_1 = \ddot{y}_2 + h_{g2} \cdot \ddot{\phi}_2, \quad X_2 = w_2 \cdot \ddot{\phi}_2, \quad X_3 = y_1 - h_{g1} \cdot \phi_1, \quad X_4 = w_1 \cdot \phi_1$$

The constants q_1 to q_4 and r are weighting factors for the state variables and control force, h_{g1} represents half of the SCM height, h_{g2} the height of the center of mass of the car body measured from the cabin floor, w_1 half of the bogie width, and w_2 half of the passenger cabin width. Specifications used in the computations are shown in Table 3.

Table 3 Parameters of criteria functions

Symbol (unit)	Value	Symbol (unit)	Value
h_{g1} (m)	0.35	h_{g2} (m)	0.45
w_1 (m)	1.57	w_2 (m)	1.20

The LQ equations are solved based on the aforementioned conditions, and u is derived using the feedback gain K which minimizes the criteria function J.

$$u = -Kx \tag{18}$$

3.3 Vibration control of the primary suspension[6]

As mentioned above, in the superconducting Maglev system, the primary suspension between the SCM and ground coils is characterized by very small passive damping. Consequently, several methods of generating electromagnetic damping forces between the SCM and ground coils are proposed.[7] In this paper, a method using a linear generator system integrated into the bogie for on-board power was examined.[8]

The bogie-integrated linear generator system generates power from relatively low speeds, and has a surplus of generated power in high speed ranges. These generator coils

serve an additional function of generating damping forces when this surplus of power is fed into the generator coils, eliminating the need for new coils solely for the purpose of generating damping forces. Furthermore, because the damping forces can be controlled electrically by the PWM converter of the linear generator device, this method has the advantage of a minimized delay in response in high frequency ranges of vibration. The magnetic fields generated in the ground coils is varied by superimposing current at frequencies matching bogie vibration on to the generator coils, and these magnetic fields can generate damping forces in the form of vertical and lateral forces and rolling moments in the SCM. Because full-scale vehicle experiments have demonstrated actual surplus of power at speeds exceeding 300 km/h, vibration control in high speed ranges is not considered to pose any problems.

The principles of the forces generated in this method have been confirmed in full-scale vehicle experiments.[9] However, because the maximum damping force that can be generated is expected to be relatively small, this paper considers an ON-OFF control that was applied as a method to maximize the effectiveness of the generated forces. The damping force generated was assumed to be ideal with no time delay. In ON-OFF control, the absolute value of the control force was kept at a constant value, and the control force was output according to the polarity of the bogie lateral speed. The generated force of only the lateral direction was used as damping force. The damping force F_m acting on the bogie can be expressed in relation to the constant magnitude of control force f_m by the following equation:

$$F_m = -sign\left(\dot{y}_1\right) \cdot f_m \qquad (19)$$

This F_m was inserted into the right-hand side of Eq. (9) in the dynamic equations of the model for the control of the secondary suspension.

Control of the primary suspension was added to the control of lateral and rolling motions in the secondary suspension (Type 2), resulting in a method labeled as control Type 3. In Type 3, the control components were designed separately for the primary and secondary suspensions.

4. Results of Simulations

4.1 Vibration control of the secondary suspension alone

(1) Control of lateral motion only (Type 1)

The effects of the control method Type 1 were examined using the weighting factors of Eq. (16) as shown in Table 4. Parameter Sets 1 and 3 consider the values of all the weighting factors to be equal, except for those corresponding to control inputs. Parameter Set 2 has large weighting factors for car body lateral and rolling-angular accelerations, while having a small weighting factor for the displacement between the bogie and guideway. Parameter Set 4 focuses on the improvement of ride comfort with respect to lateral motion.

Table 4 Weighting factors of the lateral control model (Type 1)

	q_1	q_2	q_3	q_4	r
Parameter Set 1	1.0	1.0×10^{2}	1.0×10^{4}	1.0×10^{6}	1.0×10^{-8}
Parameter Set 2	1.0×10^{2}	1.0×10^{4}	1.0×10^{2}	1.0×10^{2}	1.0×10^{-7}
Parameter Set 3	1.0	1.0×10^{2}	1.0×10^{4}	1.0×10^{6}	1.0×10^{-6}
Parameter Set 4	8.0×10^{1}	1.0×10^{1}	1.0×10^{5}	4.5×10^{6}	1.0×10^{-7}

Using the parameters in Table 4, an LQ control device was designed. The results of simulations comparing the effects of vibration control are shown in Fig. 4. The acceleration frequency responses were not much different for Parameter Sets 1 and 2 in terms of lateral and rolling motions. For Parameter Set 3, there are sharp peaks near the characteristic frequencies of each mode. For Parameter Set 4, the rolling-angular acceleration is larger

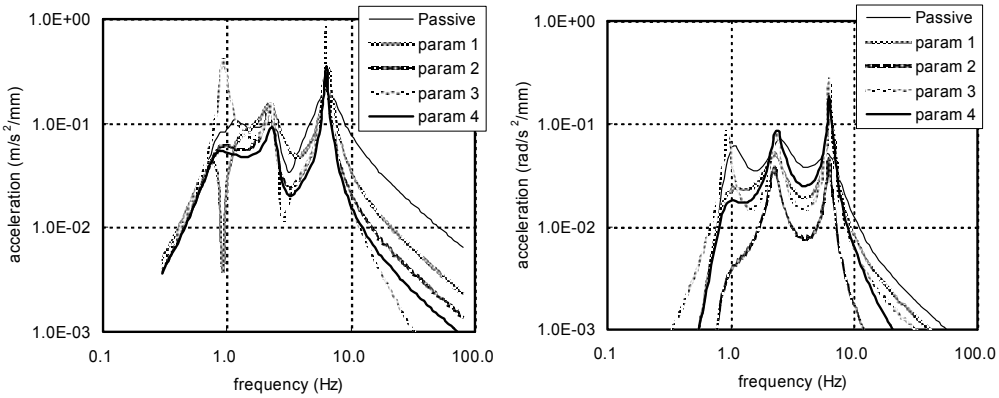

Fig. 4 Computation results for various parameters of Type-1
(left: lateral acceleration of car body, right: rolling angular acceleration of car body)

than for Parameter Sets 1 and 2, but the lateral acceleration is reduced in the range between the characteristic frequencies of the second and third modes of vibration. The weighting in this frequency range is large in the weighting curves of ISO-2631, so ride comfort with respect to lateral motion is expected to improve.

Based on these results, the weighting factors of Parameter Set 4 were used in Type 1.

(2) Control of lateral and rolling motions (Type 2)

Weighting factors that were expected to improve ride comfort with respect to lateral motion were selected for the control method Type 2, similarly to Type 1. Table 5 shows the set of weighting factors used for Type 2. Computation results of the frequency responses of car body accelerations for Type 2 using these weighting factors, plotted together with the results of Type 1, are shown in Fig. 5. The results of lateral acceleration for Type 2 generally resemble Type 1, but the peak of the third mode of vibration near 2.5 Hz is more greatly reduced, and the accelerations in the 1 to 2 Hz range were only slightly reduced compared to Type 1. Furthermore, in both Types 1 and 2, the peaks of the fourth mode of vibration near 6.5 Hz have become sharp, and the absolute values of the acceleration have become larger than in the passive case. Nevertheless, the weighting factors are small in this frequency range of the ISO-2631 weighting curves for lateral motion, and therefore are not expected to worsen the ride comfort with respect to lateral motion.

Table 5 Weighting factors of the lateral and rolling control model (Type 2)

q_1	q_2	q_3	q_4	r_l	r_v
8.0×10^{1}	1.0×10^{2}	1.0×10^{5}	4.5×10^{6}	1.0×10^{-7}	1.0×10^{-7}

The peaks of the first and second modes of vibration for the rolling-angular acceleration that could not be reduced by the control method Type 1 are greatly reduced by adding actuators for the rolling motion. Moreover, the peak of the third mode of vibration near 2.5

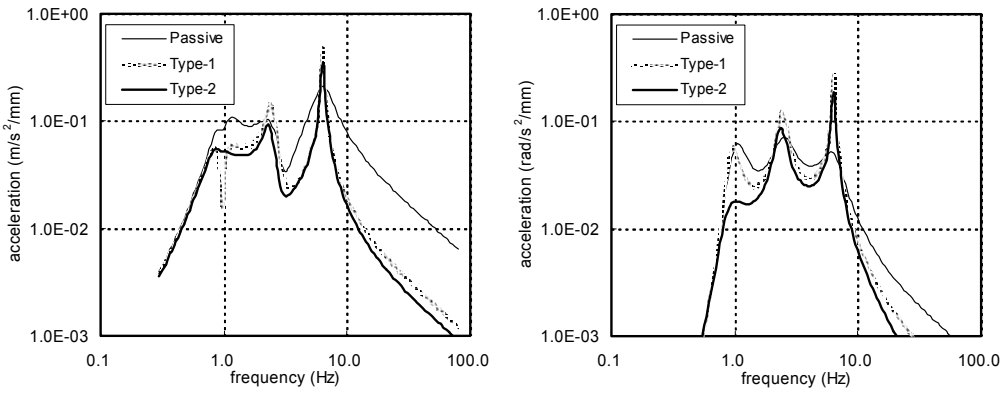

Fig. 5 Computation results of vibration control of secondary suspension alone
(left: lateral acceleration of car body, right: rolling-angular acceleration of car body)

Hz, that became larger in the control method Type 1, were restored to about the same level as that of the passive case.

The peak of the fourth mode of vibration near 6.5 Hz also became sharper for the lateral and rolling motions. However, gaps between the bogie and guideway are sufficiently large in both vertical and lateral directions, such that collisions of the vehicle against the guideway are not expected to occur for normally expected guideway irregularities.

4.2 Vibration control of both primary and secondary suspensions

(1) Effects of control methods in terms of frequency responses of accelerations

In the control method Type 3, an ideal ON-OFF control defined by Eq. (19) was applied to the primary suspension, and the LQ control of Type 2 was applied to the secondary suspension. In the primary suspension, the control force applied to the bogie was assumed to correspond to a maximum acceleration of about 0.5 m/s^2. The control of the secondary suspension included the weighting factors shown in Table 5.

A comparison of frequency responses to external disturbances with amplitudes of 1 mm for the passive case and control methods of Types 2 and 3 were plotted as shown in Fig. 6. As shown in this figure, the application of vibration control to the primary suspension resulted in a large reduction of the peak of the third mode of vibration near 2.5 Hz, for both lateral and rolling-angular accelerations. This peak is mainly a result of the bogie rolling motion with the center of rotation in the upper part of the vehicle, and the vibrations of this mode are expected to be reduced by applying control force to the lateral motion of the primary suspension. The car body lateral and rolling-angular accelerations are expected to be reduced if damping of electromagnetic forces between the bogie and guideway is feasible, even if the maximum value of the damping force is small. The effectiveness of control of the primary suspension is particularly noticeable in the frequency range of 1 to 2 Hz which is important in improving ride comfort with respect to lateral motion, which demonstrates the validity of the control method.

Furthermore, since this paper focuses on the improvement of ride comfort, no measures were taken to reduce the fourth mode of vibration near 6.5 Hz. However, this mode is characterized by a predominant rolling motion of the bogie itself, and the gain of the acceleration in this frequency range can well be reduced with the addition of damping of rolling motion in the primary suspension.

(2) Examination of the validity of frequency responses of accelerations

Because the response of control method Type 3 is non-linear, conventional linear transfer functions can not be used in the analysis. Therefore, the validity of the computations was examined using two methods of analysis described below.

(a) The time-domain response to an external disturbance in the form of a sine wave with a fixed frequency was computed for multiple cases in a range of frequencies, and the maximum amplitude at each frequency was recorded.

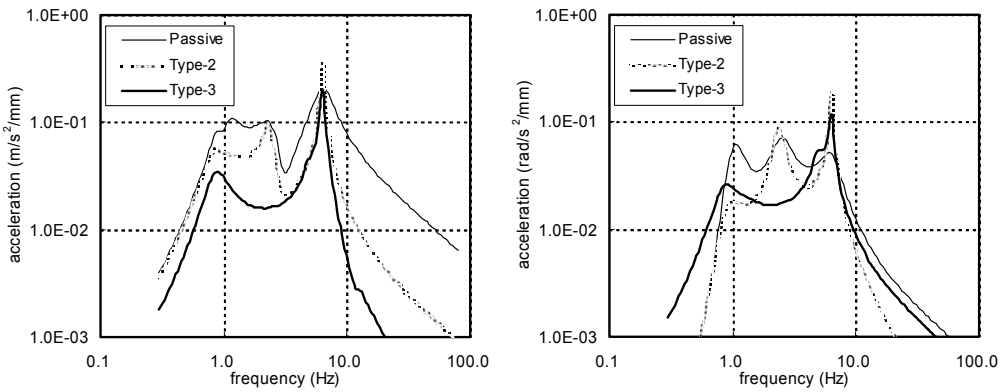

Fig. 6 Computation results of vibration control of primary and secondary suspension (left: lateral acceleration of car body, right: rolling-angular acceleration of car body)

(b) Transfer functions were derived using Laplace transforms of the dynamic equations, and the frequency response was computed using linear approximations of non-linear damping.

It is relatively easy to compute the response using method (a), but a long period of computation time is required for the transient phenomenon to converge to a stable response. And there are difficulties in the high frequency range, such as the requirement of a small time step. Considering such difficulties, method (b) was examined in the computation of the frequency response of acceleration.

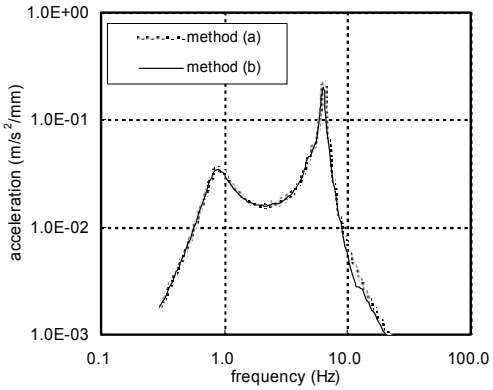

Fig. 7 Comparison of methods (a) and (b) for frequency responses of car body lateral acceleration

An example of computation results of the frequency response of car body acceleration using these two methods are shown in Fig. 7. In this figure, the frequency responses of methods (a) and (b) agree well with each other. This match demonstrates that the linear approximation method using transfer functions enables the computation of frequency response in the case of ON-OFF control, and confirms the validity of the computation model.

(3) Effects of control with respect to time-domain responses

To confirm the effectiveness of control in conditions more closely modeling actual vehicle motion, time-domain simulations were performed using modeled guideway lateral irregularities. Equation (20) is used to construct the power spectral density (PSD) of the modeled guideway irregularities.[10]

$$S(k) = A_g \cdot k^{-n} \qquad (20)$$

Here, $S(k)$ is the PSD [mm^2・m] of the guideway irregularities, and k is the wave number. The values of the parameters A_g = 0.1058 and n = 1.8 were used in this paper. These guideway irregularities were input to the model, and lateral accelerations of the car body and bogie were derived.

The results of time-domain simulations of the passive case and control method Type 3 are shown in Fig. 8. The peak of bogie acceleration was reduced to about 50% of the passive case which is about 6 m/s^2 (peak-to-peak), and the peak of the car body acceleration

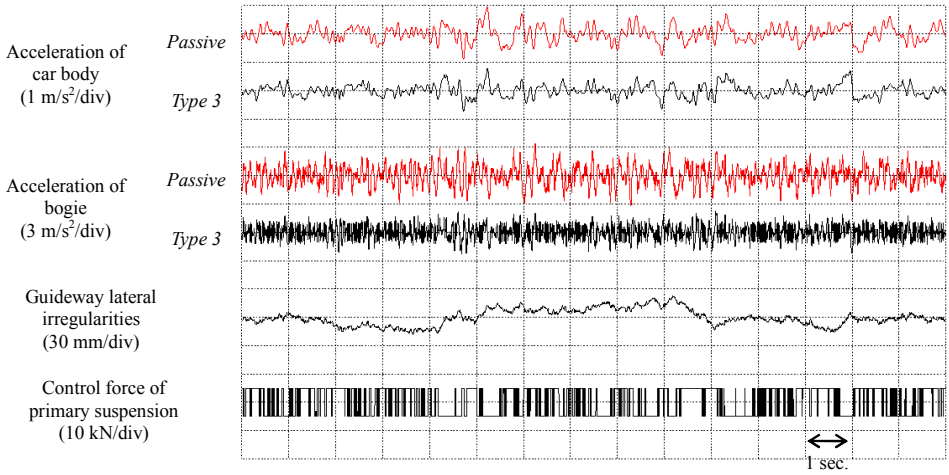

Fig. 8 Computation results of time-domain simulation

about 30% of the passive case which is about 1.5 m/s^2 (peak-to-peak). In terms of zero-to-peak values, the bogie acceleration was reduced to about 35% of the passive case, and the car body acceleration about 25% of the passive case, demonstrating the effectiveness of applying vibration control. The direction of the control force plotted in this figure is shown to fluctuate according to the polarity of the bogie velocity.

5. Conclusions

With the objective of improving ride comfort of Maglev vehicles with respect to lateral and rolling motions, simulations were performed to estimate the effectiveness of control methods, with an LQ control using active suspension applied to the secondary suspension, and an ON-OFF control using forces generated by a linear generator system integrated into an existing bogie applied to the primary suspension.

Results indicated that the control of the secondary suspension alone is effective in controlling the first and second modes of vibration, but limited in effectiveness of vibration control at frequencies higher than these two modes. By applying vibration control to the primary suspension in addition to control of the secondary suspension, vibrations of the third mode were greatly reduced, demonstrating the effectiveness of vibration control in a wider range of frequencies.

References

(1) Yoshioka, H. and Miyamoto, M., Dynamic characteristics of Maglev vehicle MLU001 - guideway irregularity test, *International Conference of Magnetically Levitated Systems & Linear Drives*, (1986-5), pp. 89-94.

(2) Yoshioka, H., Dynamic model of Maglev vehicle, *Railway Technical Research Institute (RTRI) Report*, Vol. 2, No. 6, (1988-6), pp. 17-22 *(in Japanese)*.

(3) Yoshioka, H. and Watanabe, K., Dynamic characteristics of a sidewall magnetically levitated vehicle, *Railway Technical Research Institute (RTRI) Report*, Vol. 8, No. 10, (1994-10), pp. 29-34 *(in Japanese)*.

(4) Azakami, M., The development of Maglev bogie system on the first train set for Yamanashi Test Line, *Railway Technical Research Institute (RTRI) Report*, Vol. 10, No. 1, (1996-1), pp. 11-16 *(in Japanese)*.

(5) Watanabe, K., Ohta, Y., Nagai, M., and Kamada, T., A study of the vibration analysis of a Maglev vehicle, *10th International Symposium on Applied Electromagnetics and Mechanics*, (2001-5), pp. 47-48.

(6) Watanabe, K., Yoshioka, H., Watanabe, E., Tohtake, T., and Nagai, M., A study of the vibration control system for a superconducting Maglev vehicle, *6th International Conference on Motion and Vibration Control*, (2002-8), pp. 907-912.

(7) Azuma, K., Ohashi, S., Ohsaki, H., and Masada, E., Magnetic damping of the electromagnetic suspension type superconducting levitation system, *Institute of Electrical Engineers of Japan (IEEJ) Transactions on Industry Applications*, Vol. 117-D, No. 8, (1997-8), pp. 1015-1023 *(in Japanese)*.

(8) Murai, T., Hasegawa, H., Yamamoto, T., and Fujiwara, S., Active magnetic damper using linear generator, *Institute of Electrical Engineers of Japan (IEEJ) Transactions on Industry Applications*, Vol. 119-D, No. 11, (1999-11), pp. 1371-1376 *(in Japanese)*.

(9) Hasegawa, H., Murai, T., and Yamamoto, T., Running tests of a combined SC type linear generator, *Institute of Electrical Engineers of Japan (IEEJ) Transactions on Industry Applications*, Vol. 123-D, No. 2, (2003-2), pp. 156-163 *(in Japanese)*.

(10) Furukawa, A. and Hashimoto, S., Power spectrum density of Maglev guideway irregularity and riding quality level, *Railway Technical Research Institute (RTRI) Report*, Vol. 7, No. 2, (1993-2), pp. 11-18 *(in Japanese)*.